HOT-ELECTRON INVESTIGATION IN SEMICONDUCTOR DEVICES USING A MULTIDIMENSIONAL SPHERICAL HARMONICS EXPANSION OF THE BOLTZMANN TRANSPORT EQUATION *

G. Baccarani, A. Gnudi, D. Ventura
University of Bologna, Department of Electronics
viale Risorgimento 2, 40136 Bologna, Italy

Abstract

Two applications of the spherical harmonics expansion method of the Boltzmann Transport Equation (BTE) are presented. First, the carrier energy spectrum of a two-dimensional MOSFET up to 2.6 eV is investigated. The model includes phonon and ionized impurity scattering as well as a system of non-parabolic bands. Then impact ionization is added to the model to simulate a one-dimensional BJT and to calculate the collector current multiplication factor.

Introduction

Semiconductor device simulation is traditionally based either on expansions in the carrier distribution momenta (drift-diffusion and hydrodynamic models), or on particle methods (Monte Carlo). The spherical harmonics expansion technique [1, 2, 3] lies between these two approaches, since it is more accurate than the methods of the first type and less CPU intensive than Monte Carlo. The main idea is to reduce the dimensionality of the problem by expanding the distribution function into a series of spherical harmonics in the momentum space. A new set of unknowns is obtained, i.e. the coefficients of the expansion, which depend on the physical space (x, y, z) and on the modulus of the momentum only.
The multidimensional formulation of the problem and the implementation up to the two-dimensional real space case have been already carried out and the results presented elsewhere [4, 5].
In this note we briefly review two applications of the model: the investigation of the electron transport in a two-dimensional cross-section of a MOSFET, and the one-dimensional simulation of a BJT including impact ionization. From these preliminary tests the model appears very attractive, combining computational efficiency with adequate physical description.

The mathematical model

We refer the readers to [4] for the details of the mathematical model. In this section we report the key points of the procedure.
Consider the classical stationary, linear BTE for electrons in the conduction band

$$\mathbf{u}_g(\mathbf{k}) \cdot \nabla_{\mathbf{r}} f(\mathbf{r},\mathbf{k}) - \frac{q}{h}\,\mathbf{F}(\mathbf{r}) \cdot \nabla_{\mathbf{k}} f(\mathbf{r},\mathbf{k}) =$$

$$\int S(\mathbf{k}',\mathbf{k})\, f(\mathbf{r},\mathbf{k}')\, \mathrm{d}^3k' - f(\mathbf{r},\mathbf{k}) \int S(\mathbf{k},\mathbf{k}')\, \mathrm{d}^3k' \qquad (1)$$

*This research was supported by IBM, General-Technology Division, Essex Junction VT, 05452 - USA

where $\mathbf{u}_g$ is the group velocity, $S(\mathbf{k},\mathbf{k}')$ the differential electron scattering probability per unit time from state $\mathbf{k}$ to state $\mathbf{k}'$, and $f(\mathbf{r},\mathbf{k})$ the electron distribution function. In Eq. (1), the exclusion principle and electron-electron scattering, which make the collision operator non linear, are neglected. We expand f as

$$f(\mathbf{r},\mathbf{k}) = f_0(\mathbf{r},k) + \frac{k_i}{k} f_i(\mathbf{r},k) + \frac{1}{2}\frac{k_i}{k}\frac{k_j}{k} f_{ij}(\mathbf{r},k) + \ldots \tag{2}$$

where $i,j = 1..3$, and f_{ij} is a traceless tensor. Summation over repeated indices is assumed here and in the following expressions. Expression (2) is equivalent to a spherical harmonics expansion of f in the momentum space.

The matrix $S(\mathbf{k}',\mathbf{k})$ of the most effective scattering mechanisms in silicon (acoustic phonon, optical phonon, and ionized impurity scattering) depends only on the moduli of the vectors $\mathbf{k}$ and $\mathbf{k}'$ and the angle ξ between them. Therefore we expand it as

$$S(\mathbf{k}',\mathbf{k}) = S_0(k',k) + S_1(k',k)\frac{k_i}{k}\frac{k_i'}{k} + S_2(k',k)\frac{1}{2}(3\frac{k_i}{k}\frac{k_i'}{k}\frac{k_j}{k}\frac{k_j'}{k} - 1) + \ldots \tag{3}$$

where $(k_i k_i')/k^2 = \cos\xi$.

The scattering matrix for impact ionization, in the Born approximation, is

$$S^{ii}(\mathbf{k},\mathbf{k}',\mathbf{k}'') = b_{ii}[a^2 + (\mathbf{k}'-\mathbf{k})^2)]^{-2}\,\delta(E - E' - E'' - E_G) \tag{4}$$

where $\mathbf{k}$ and $\mathbf{k}'$ are the initial and final states of the ionizing electron, $\mathbf{k}''$ is the final state of the electron coming from the valence band, b_{ii} a normalizing constant, E_G the energy gap and a the inverse screening length. In the derivation of Eq. 4 we assumed flat valence band and occupation probability of the valence band equal to one. The following definitions are also useful:

$$A(E',E) = \int g(E'')[S_0^{ii}(E',E,E'') + S_0^{ii}(E',E'',E)]\mathrm{d}E'' \tag{5.a}$$

$$B(E',E) = \int g(E'')S_1^{ii}(E',E,E'')\mathrm{d}E'' \tag{5.b}$$

where S_0^{ii} and S_1^{ii} are the first two coefficients of an expansion of (4) similar to (3).

Replacement of (2) and (3) together with the expansion of (4) into the BTE (1) and matching harmonic terms of equal order yields an infinite set of PDEs in the unknown coefficients $f_0, f_i, f_{ij}, \ldots$. In order to obtain a closed system of equations a truncation is necessary. In the simulations presented in this paper we keep only the lowest-order terms in f_0 and f_i. The error due to this truncation for the spatially uniform problem is discussed in [3]. The additional assumption we need is the spherical symmetry of the energy/wave-vector dispersion relation of the conduction band. It has been shown that this does not represent a serious limit to the accurate description of electron transport [6].

If the coordinate transformation $(\mathbf{r},k) \rightarrow (\mathbf{r},H)$ is applied, where $H = E(k) - q\psi(\mathbf{r})$ is the electron total energy, the resulting system of equations turns out to be (see [4] and [5]):

$$\frac{\partial}{\partial r_i}\left[g\,u_g\lambda\frac{\partial f_0}{\partial r_i} - \frac{g\lambda}{3}\int B(H',H)\,f_i(H')\,g(H')\,\mathrm{d}H'\right] + 3c_{op}\,g\Big\{g^+\left[N_{op}^+ f_o^+ - N_{op}f_o\right] - \tag{6.a}$$

$$-g^-\left[N_{op}^+ f_0 - N_{op}f_0^-\right]\Big\} - 3\,g^2 c_{ii}\,f_0 + 3\,g\int A(H',H)f_0(H')\,g(H')\,\mathrm{d}H' = 0$$

$$f_i = -\lambda\frac{\partial f_0}{\partial r_i} + \frac{\lambda}{3u_g}\int B(H',H)\,f_i(H')\,g(H')\,\mathrm{d}H' \tag{6.b}$$

In Eqs. (6) acoustic and optical phonon scattering, ionized impurity scattering as well as impact ionization are considered. The parameter c_{op} depends on the optical phonon coupling constant, N_{op} and $\hbar\omega_{op}$ are the optical phonon occupation number and energy respectively, $N_{op}^{+} = N_{op} + 1$. The form of the band structure is defined implicitly by the relation $\gamma(E) = (\hbar^2 k^2)/(2m^*)$, where $\gamma(E)$ is a suitable function. The density of states g and the group velocity u_g are related to γ by $g = 2\pi(2m^*/h^2)^{3/2}\gamma^{1/2}\gamma'$, $u_g = (2/m^*)^{1/2}\gamma^{1/2}/\gamma'$. We have also defined $g^{\pm}(H) = g(H \pm \hbar\omega_{op})$, and similarly $f_0^{\pm}$. In the above equations $\lambda(E)$ is the total carrier mean free path

$$\lambda(E) = \frac{u_g(E)}{c_{ac}\, g(E) + c_{op}\, N_{op}^{+}\, g^{-}(E) + c_{op}\, N_{op}\, g^{+}(E) + [c_i(E, N_i) + c_{ii}(E)]\, g(E)} \tag{7}$$

In (6) and (7) c_i and c_{ii} are the effective impurity scattering probability and the total impact ionization scattering probability respectively.

The band structure and the parameters for the scattering rates have been taken from [6]. We used only the two lowest bands of [6], with which the experimental density of states is correctly accounted for up to 2.6 eV, enough for the purpose of modeling impact ionization. Notice that the lowest band is non-parabolic ($\gamma(E) = E(1+\alpha E)$), whereas the upper band is parabolic ($\gamma(E) = E$). Apart from the integral terms, Eq. (6,a) is a second order linear difference-differential equation with non-constant coefficients. In the 2-D real space case the equation must be solved on the three-dimensional domain (x, y, H) with boundary surfaces $(x, y) \in \Gamma$, $H = -q\psi(x, y)$, $H = E_{max} - q\psi(x, y)$, where Γ is the boundary of the device cross-section, and E_{max} is the maximum energy of our band system. Equilibrium distributions for f_0 are assumed at the ohmic contacts, whereas Neumann conditions are imposed at the free boundaries. At the energy extrema $E = 0$ and $E = E_{max}$ regularity of the solution is required by symmetry considerations in the $\mathbf{k}$ space. The integral terms are actually considered in the calculations by means of an iterative procedure. The convergence rate is usually very fast.

MOSFET simulation

The model presented in the previous section was applied to the simulation of a two-dimensional n-channel MOSFET with a $10^{17}\,\mathrm{cm}^{-3}$ bulk doping concentration, a gaussian p-type channel implant with a $2 \times 10^{17}\,\mathrm{cm}^{-3}$ peak located at the surface and a $0.04\,\mu$m standard deviation. The channel length was $0.33\,\mu$m, the junction depth $0.11\,\mu$m and the oxide thickness 7 nm. The simulation was performed with $V_{GS} = V_{DS} = 3\,\mathrm{V}$. Impact ionization was neglected in this 2-D simulation. It was instead considered for the simulation of the BJT presented in the next paragraph.

The electric potential was calculated from the solution of the hydrodynamic model coupled with the Poisson equation. The hydrodynamic transport parameters (electron mobility and energy-relaxation time) have been tuned on the homogeneous bulk material.

The discretization grid contained about 1,300 nodes in the (x, y) plane, and 580 nodes in the energy direction H. The linear systems were solved by means of a *CGS* solver [7]. A complete run on an IBM RS/6000-320 workstation required about 90 minutes of CPU time.

In Fig. 1 we show a logarithmic plot of the f_0 component of the expansion. Notice that f_0 is the integral of the distribution function over the solid angle, and therefore represents the energy distribution of electrons. The front plane ($E = 0$) corresponds to the geometrical cross-section of the device. Since the electron density is given by $n = \int f_0 g dE$ and f_0 is a fast decaying function in energy, $f_0(x, y, 0)$ is roughly proportional to n. The highly doped source and drain neutral regions, together with the inversion layer, are clearly identifiable. Equilibrium Boltzmann distribution is forced at the source and drain contacts, resulting in uniformly spaced grey tones. At the drain end

of the channel the strong heating of the electrons accelerated by the electric field is indicated by the darker region in the high-energy portion of the plot.
Fig. 2 represents a plane section of the previous plot cut at the depth of 547 Å below the interface. Electrons are in equilibrium within the source, as indicated by the constant slope. In the channel region the high-energy tail becomes increasingly more populated as electrons move toward the drain. Two populations seem to coexist within the drain region, as revealed by the two different slopes of the distribution at high and low energies: hot electrons which have travelled across the channel and majority carriers in quasi-equilibrium conditions. The tail of the distribution decays slowly as electrons move leftward. The distribution is still off-equilibrium when electrons hit the free boundary on the left. This is likely to be an unphysical effect due to the neglect of electron-electron interaction and impact-ionization, which are known to push the distribution toward local equilibrium.

Simulation of the BJT including impact ionization.

We performed the simulation of the one-dimensional *n-p-n* bipolar device described in [8] including impact ionization.
In Fig. 3 the ionization coefficient α, defined as $\alpha = (nv)^{-1} \int f_0 c_{ii} g^2 \, dE$ obtained from a homogeneous simulation as a function of the inverse electric field is compared with the experimental data of Van Overstraeten and Lee, as well as with Monte Carlo results from [9].
The current multiplication factor $M - 1 = (J_{out} - J_{in})/J_{in}$ is shown in Fig. 4 against V_{CB} for three different values of the collector doping concentration. We want to stress that no fitting parameter has been adjusted, and yet a reasonable qualitative agreement with experiment was obtained. The quantitative differences may be due to a number of reasons, including the uncertainty in the doping profiles.

Acknowledgments.

The authors are grateful to the memory of Dr. F. Odeh for many helpful discussions.

References

[1] N. Goldsman et al., J. Appl. Phys., vol. 68, no. 3, p. 1075, 1990

[2] N. Goldsman et al., Solid-St. Electron., vol. 34, no. 4, p. 389, 1991

[3] D. Ventura et al., IEICE Trans. Electron., vol. E75-C, no. 2, p. 194, 1992

[4] D. Ventura et al., Appl. Math. Lett., vol. 5, no. 3, p. 85, 1992

[5] A. Gnudi et al., Proc. of the SISDEP '91 Conf., p. 205, September 1991, Zurich

[6] R. Brunetti et al., Solid-St. Electron., vol. 32, no. 12, p. 1663, 1989

[7] P. Sonneveld, SIAM J. Sci. Stat. Comput. vol. 10, no. 1, p. 36, 1989

[8] E. F. Crabbé et al., IEDM-90 Tech. Dig., pp. 463–466, 1990

[9] R. Thoma et al., J. Appl. Phys., vol. 69, no. 4, p. 2300, 1991

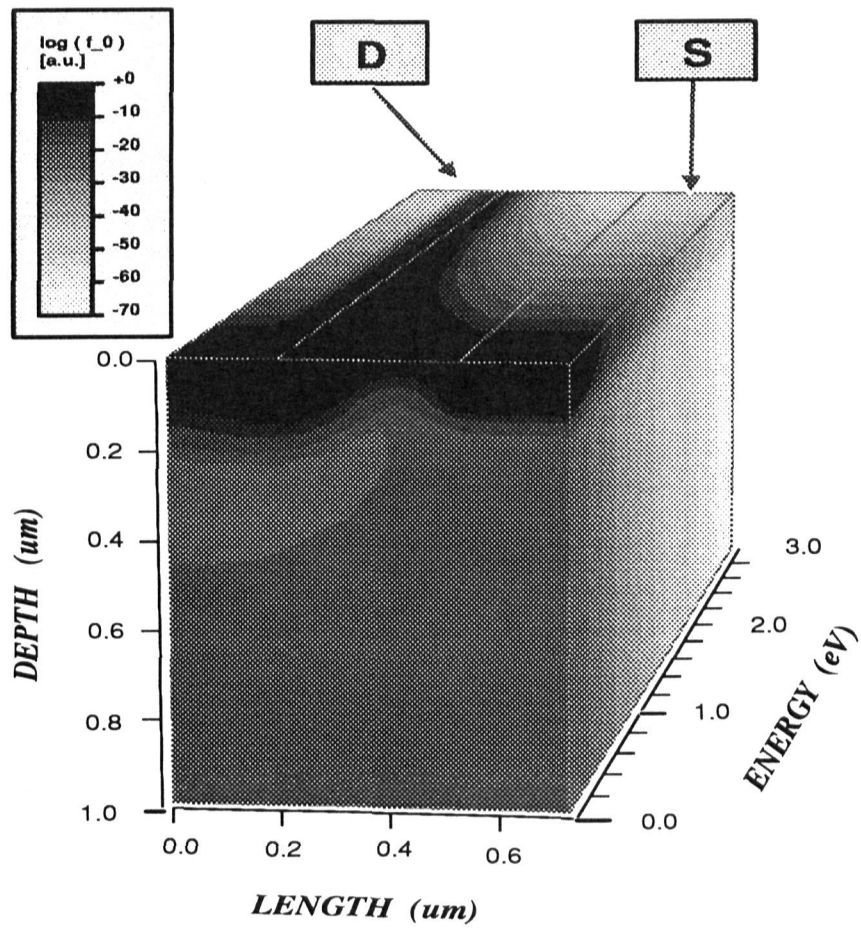

Fig. 1. Electron energy distribution.

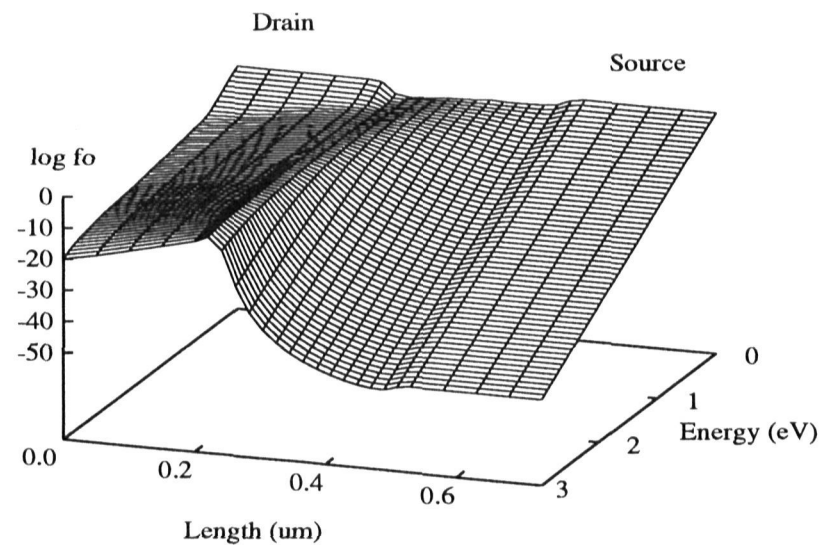

Fig. 2. Electron energy distribution along a horizontal line located at 547 Å below the interface.

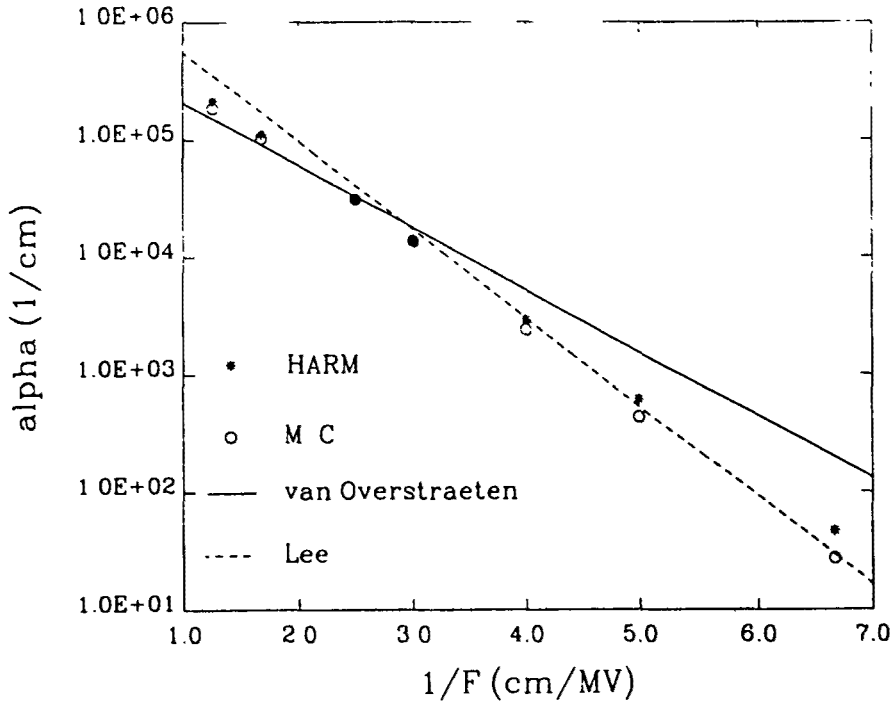

Fig. 3. Ionization coefficient vs. inverse electric field from the present model compared with experimental data.

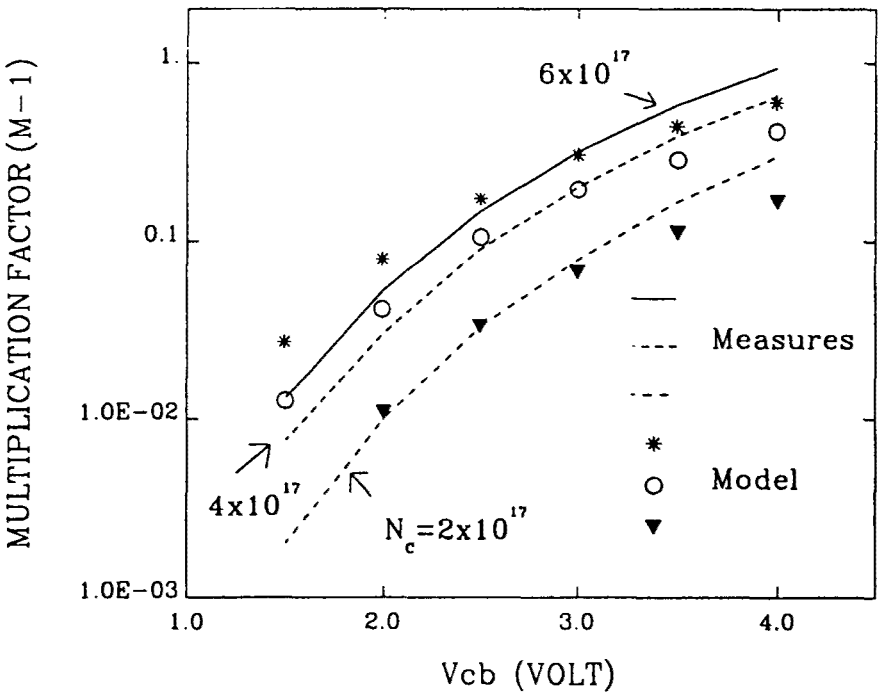

Fig. 4. Collector current multiplication factor compared with experimental data at various doping concentration.